RECOMMENDATION ITU-R P.531-5

IONOSPHERIC PROPAGATION DATA AND PREDICTION METHODS REQUIRED FOR THE DESIGN OF SATELLITE SERVICES AND SYSTEMS

(Question ITU-R 218/3)

(1978-1990-1992-1994-1997-1999)

The ITU Radiocommunication Assembly,

considering

a) that the ionosphere causes significant propagation effects at frequencies up to at least 12 GHz;

b) that effects may be particularly significant for non-geostationary-satellite orbit services below 3 GHz;

c) that experimental data have been presented and/or modelling methods have been developed that allow the prediction of the ionospheric propagation parameters needed in planning satellite systems;

d) that ionospheric effects may influence the design and performance of integrated services digital network (ISDN) and other radio systems involving spacecraft;

e) that these data and methods have been found to be applicable, within the natural variability of propagation phenomena, for applications in satellite system planning,

recommends

1 that the data prepared and methods developed as set out in Annex 1 be adopted for planning satellite systems, in the respective ranges of validity indicated in the Annex 1.

ANNEX 1

1 Introduction

This Annex deals with the ionospheric propagation effects on Earth-space paths. From a system design viewpoint, the impact of ionospheric effects can be summarized as follows:

a) the total electron content (TEC) accumulated along a mobile-satellite service (MSS) transmission path penetrating the ionosphere causes rotation of the polarization (Faraday rotation) of the MSS carrier and time delay of the signal, and a change in the apparent direction of arrival due to refraction;

b) localized random ionospheric patches, commonly referred to as ionospheric irregularities, further cause excess and random rotations and time delays, which can only be described in stochastic terms;

c) because the rotations and time delays relating to electron density are non-linearly frequency dependent, and because localized ionospheric irregularities apparently move in and out of the link path which cause Doppler effects, both § a) and b) further result in dispersion or group velocity distortion of the MSS carriers;

d) furthermore, localized ionospheric irregularities also act like convergent and divergent lens which focus and defocus the radio waves. Such effects are commonly referred to as the scintillations which affect amplitude, phase and angle-of-arrival of the MSS signal.

Due to the complex nature of ionospheric physics, system parameters affected by ionospheric effects as noted above cannot always be succinctly summarized in simple analytic formulae. Relevant data edited in terms of tables and/or graphs, supplemented with further descriptive or qualifying statements, are for all practical purposes the best way to present the effects.

In considering propagation effects in the design of MSS at frequencies below 3 GHz, one has to recognize that:

e) the normally known space-Earth propagation effects caused by hydrometeors are not significant relative to effects of § f) and h);

f) the near surface multipath effects, in the presence of natural or man-made obstacles and/or at low elevation angles, are always critical;

g) the near surface multipath effects vary from locality to locality, and therefore they do not dominate the overall design of the MSS system when global scale propagation factors are to be dealt with;

h) ionospheric effects are the most significant propagation effects to be considered in the MSS system design in global scale considerations.

2 Background

Caused by solar radiation, the Earth's ionosphere consists of several regions of ionization. For all practical communications purposes, regions of the ionosphere, D, E, F and top-side ionization have been identified as contributing to the TEC between satellite and ground terminals.

In each region, the ionized medium is neither homogeneous in space nor stationary in time. Generally speaking, the background ionization has relatively regular diurnal, seasonal and 11-year solar cycle variations, and is dependent strongly on geographical locations and geomagnetic activity. In addition to the background ionization, there are always highly dynamic, small-scale non-stationary structures known as irregularities. Both the background ionization and irregularities degrade radiowaves. Furthermore, in the background ionization and irregularities cause the refractive index to become frequency dependent, i.e. the medium is dispersive.

3 Prime degradations due to background ionizations

A number of effects, such as refraction, dispersion and group delay, are in magnitude directly proportional to the TEC; Faraday rotation is also approximately proportional to TEC, with the contributions from different parts of the ray path weighted by the longitudinal component of magnetic field. A knowledge of the TEC thus enables many important ionospheric effects to be estimated quantitatively.

3.1 TEC

Denoted as N_T, the TEC can be evaluated by:

$$N_T = \int_s n_e(s)\, \mathrm{d}s \tag{1}$$

where:

s: propagation path (m)

n_e: electron concentration (el/m^3).

Even when the precise propagation path is known, the evaluation of N_T is difficult because n_e has diurnal, seasonal and solar cycle variations.

For modelling purposes, the TEC value is usually quoted for a zenith path having a cross-section of 1 m^2. The TEC of this vertical column can vary between 10^{16} and 10^{18} el/m^2 with the peak occurring during the sunlit portion of the day. From a knowledge of the TEC, Faraday rotation and group delay can be estimated for communications applications. The estimate is provided below.

The standard monthly median ionosphere is the COSPAR-URSI International Reference Ionosphere IRI-90. Although there are no analytical expressions available for integration of this model, under conditions of low to moderate solar activity numerical techniques may be used to derive values for any location, time and chosen set of heights up to 1 000 km. Under conditions of high solar activity, problems may arise with values of electron content derived

from IRI-90. For many purposes it is sufficient to estimate electron content by multiplication of the peak electron density with an equivalent slab thickness value of 300 km. Where instantaneous values are required, real-time data may be obtained, for example, using signals from the global positioning system (GPS).

3.2 Faraday rotation

When propagating through the ionosphere, a linearly polarized wave will suffer a gradual rotation of its plane of polarization due to the presence of the geomagnetic field and the anisotropy of the plasma medium. The magnitude of Faraday rotation, θ, will depend on the frequency of the radiowave, the magnetic field strength, and the electron density of the plasma as:

$$\theta = 2.36 \times 10^2 \; B_{av} \; N_T \; f^{-2} \tag{2}$$

where:

θ: angle of rotation (rad)

B_{av}: average Earth magnetic field (Wb/m^2)

f: frequency (GHz)

N_T: TEC (el/m^2).

Typical values of θ are shown in Fig. 1.

FIGURE 1

Faraday rotation as a function of TEC and frequency

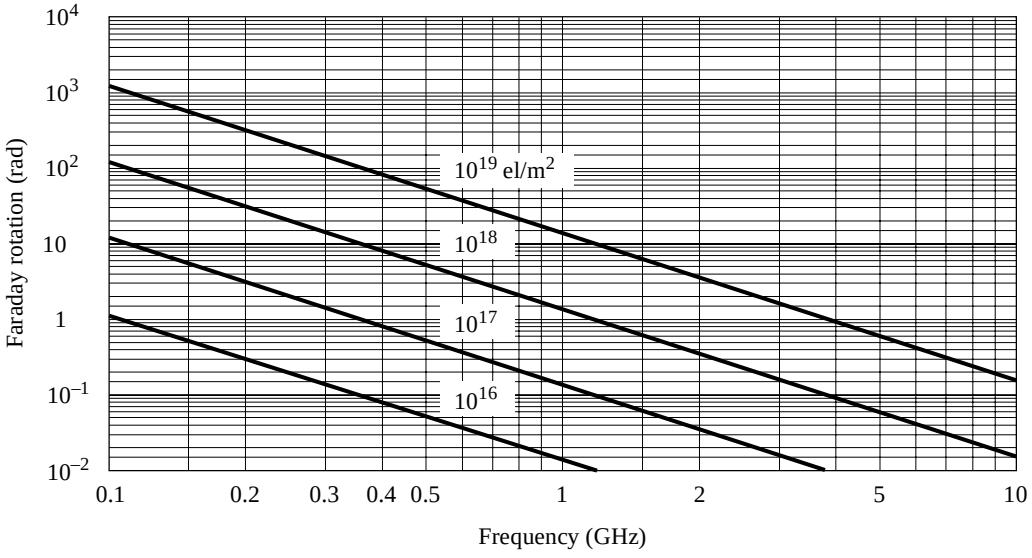

0531-01

The Faraday rotation is thus inversely proportional to the square of frequency and directly proportional to the integrated product of the electron density and the component of the Earth's magnetic field along the propagation path. Its median value at a given frequency exhibits a very regular diurnal, seasonal, and solar cyclical behaviour that can be predicted. This regular component of the Faraday rotation can therefore be compensated for by a manual adjustment of the polarization tilt angle at the earth-station antennas. However, large deviations from this regular behaviour can occur for small percentages of the time as a result of geomagnetic storms and, to a lesser extent, large-scale travelling ionospheric disturbances. These deviations cannot be predicted in advance. Intense and fast fluctuations of the Faraday rotation angles of VHF signals have been associated with strong and fast amplitude scintillations respectively, at locations situated near the crests of the equatorial anomaly.

The cross-polarization discrimination for aligned antennas, XPD (dB), is related to the Faraday rotation angle, θ, by:

$$XPD = -20 \log (\tan \theta) \quad (3)$$

3.3 Group delay

The presence of charged particles in the ionosphere slows down the propagation of radio signals along the path. The time delay in excess of the propagation time in free space, commonly denoted as *t*, is called the group delay. It is an important factor to be considered for MSS systems. This quantity can be computed as follows:

$$t = 1.345\, N_T / f^2 \times 10^{-7} \quad (4)$$

where:

t: delay time (s) with reference to propagation in a vacuum

f: frequency of propagation (Hz)

N_T: determined along the slant propagation path.

Figure 2 is a plot of time delay, *t*, versus frequency, *f*, for several values of electron content along the ray path.

FIGURE 2

Ionospheric time delay versus frequency for various values of electron content

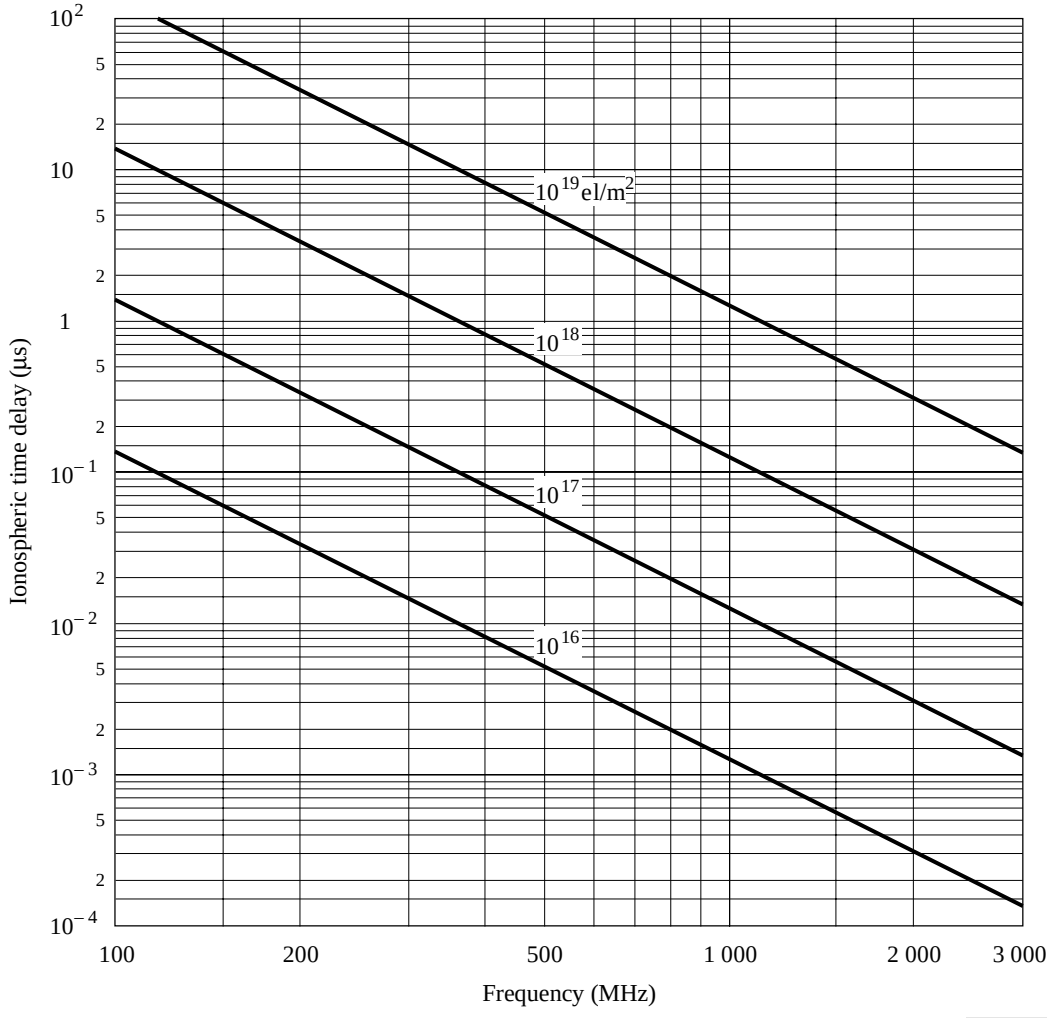

For a band of frequencies around 1 600 MHz the signal group delay varies from approximately 0.5 to 500 ns, for TEC from 10^{16} to 10^{19} el/m^2. Figure 3 shows the yearly percentage of daytime hours that the time delay will exceed 20 ns at a period of relatively high solar activity.

FIGURE 3

Contours of percentage of yearly average daytime hours when time delay at vertical incidence at 1.6 GHz exceeds 20 ns (sunspot number = 140)

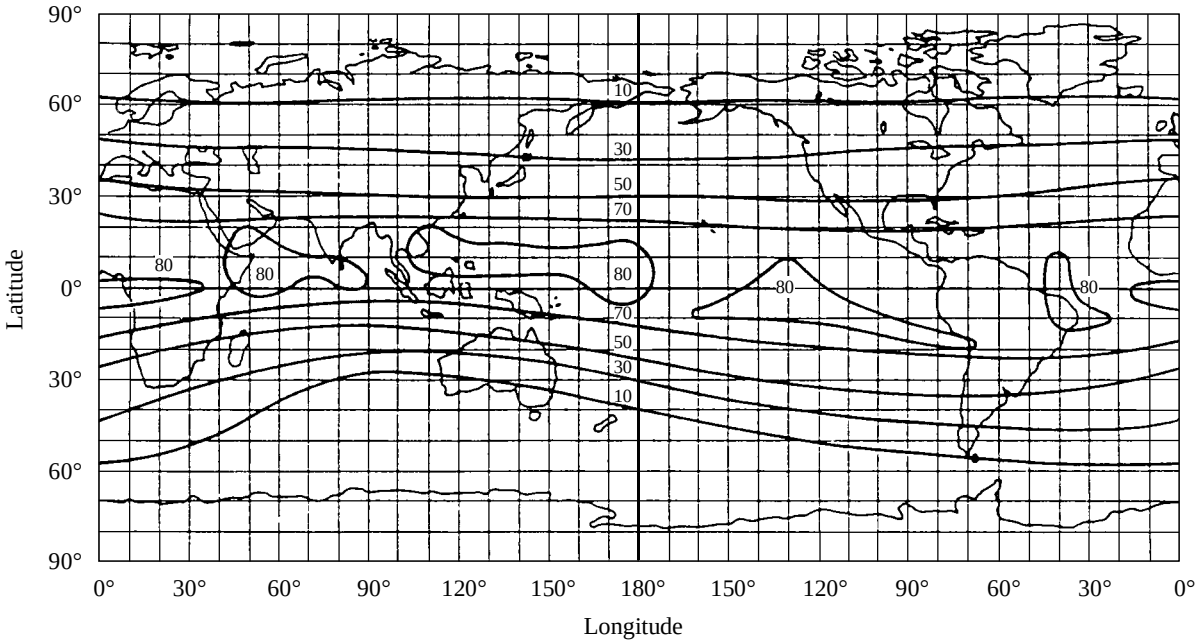

3.4 Dispersion

When trans-ionospheric signals occupy a significant bandwidth the propagation delay (being a function of frequency) introduces dispersion. The differential delay across the bandwidth is proportional to the integrated electron density along the ray path. For a fixed bandwidth the relative dispersion is inversely proportional to frequency cubed. Thus, systems involving wideband transmissions must take this effect into account at VHF and possibly UHF. For example, as shown in Fig. 4 for an integrated electron content of 5×10^{17} el/m^2, a signal with a pulse length of 1 μs will sustain a differential delay of 0.02 μs at 200 MHz while at 600 MHz the delay would be only 0.00074 μs (see Fig. 4).

3.5 TEC rate of change

With an orbiting satellite the observed rate of change of TEC is due in part to the change of direction of the ray path and in part to a change in the ionosphere itself. For a satellite at a height of 22 000 km traversing the auroral zone, a maximum rate of change of 0.7×10^{16} el/m^2/s has been observed. For navigation purposes, such a rate of change corresponds to an apparent velocity of 0.11 m/s.

4 Principal degradation due to irregularities

4.1 Scintillation

One of the most severe disruptions along a trans-ionospheric propagation path for signals below 3 GHz is caused by ionospheric scintillation. Principally through the mechanisms of forward scattering and diffraction, small-scale irregular structures in the ionization density cause scintillation phenomena in which the steady signal at the receiver is replaced by

one which is fluctuating in amplitude, phase and apparent direction of arrival. Depending on the modulation of the system, various aspects of scintillation affect the system performance differently. The most commonly used parameter characterizing the intensity fluctuations is the scintillation index S_4, defined by equation (5):

$$S_4 = \left(\frac{\left\langle I^2 \right\rangle - \left\langle I \right\rangle^2}{\left\langle I \right\rangle^2} \right)^{1/2} \tag{5}$$

where I is the intensity of the signal and $\left\langle \ \right\rangle$ denotes averaging.

The scintillation index S_4 is related to the peak-to-peak fluctuations of the intensity. The exact relationship depends on the distribution of the intensity. The intensity distribution is best described by the Nakagami distribution for a wide range of S_4 values. As S_4 approaches 1.0, the distribution approaches the Rayleigh distribution. Occasionally, S_4 may exceed 1, reaching values as high as 1.5. This is due to wave focusing caused by the irregularities. For values less than 0.6, S_4 shows a consistent $f^{-\upsilon}$ relationship, with υ the spectral index being 1.5, for most multifrequency observations in the VHF and UHF bands. Many equatorial observations at gigahertz frequencies, however, suggest values higher than 1.5. for the spectral index. As the scintillation becomes stronger, with S_4 exceeding 0.6, the spectral index decreases. This is due to the saturation of scintillation for Rayleigh fading under the strong influence of multiple scattering.

FIGURE 4

Difference in the time delay between the lower and upper frequencies of the spectrum of a pulse of width, τ, transmitted through the ionosphere, one way traversal

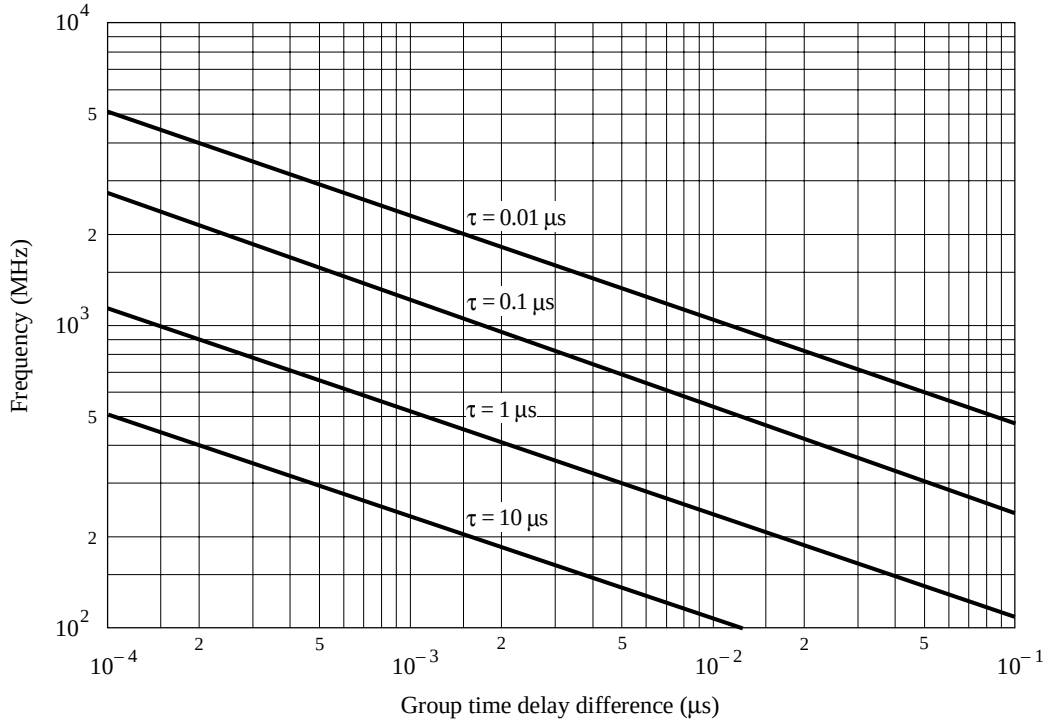

Empirically, Table 1 provides a convenient conversion between S_4 and the approximate peak-to-peak fluctuations P_{fluc} (dB). This relationship can be approximated by:

$$P_{fluc} = 27.5\ S_4^{1.26} \tag{6}$$

TABLE 1

Empirical conversion table for scintillation indices

S_4	P_{fluc} (dB)
0.1	1.5
0.2	3.5
0.3	6
0.4	8.5
0.5	11
0.6	14
0.7	17
0.8	20
0.9	24
1.0	27.5

4.2 Geographic, equinoctial and solar dependence of scintillations

Geographically, there are two intense zones of scintillation, one at high latitudes and the other centred within ± 20° of the magnetic equator as shown in Fig. 5. Severe scintillation has been observed up to gigahertz frequencies in these two sectors, while in the middle latitudes scintillation mainly affects VHF signals. In all sectors, there is a pronounced night-time maximum of activity as also indicated in Fig. 5. For equatorial gigahertz scintillation, peak activity around the vernal equinox and high activity at the autumnal equinox have been observed.

FIGURE 5

Depth of scintillation fading (proportional to density of cross-hatching) at L-band during solar maximum and minimum years

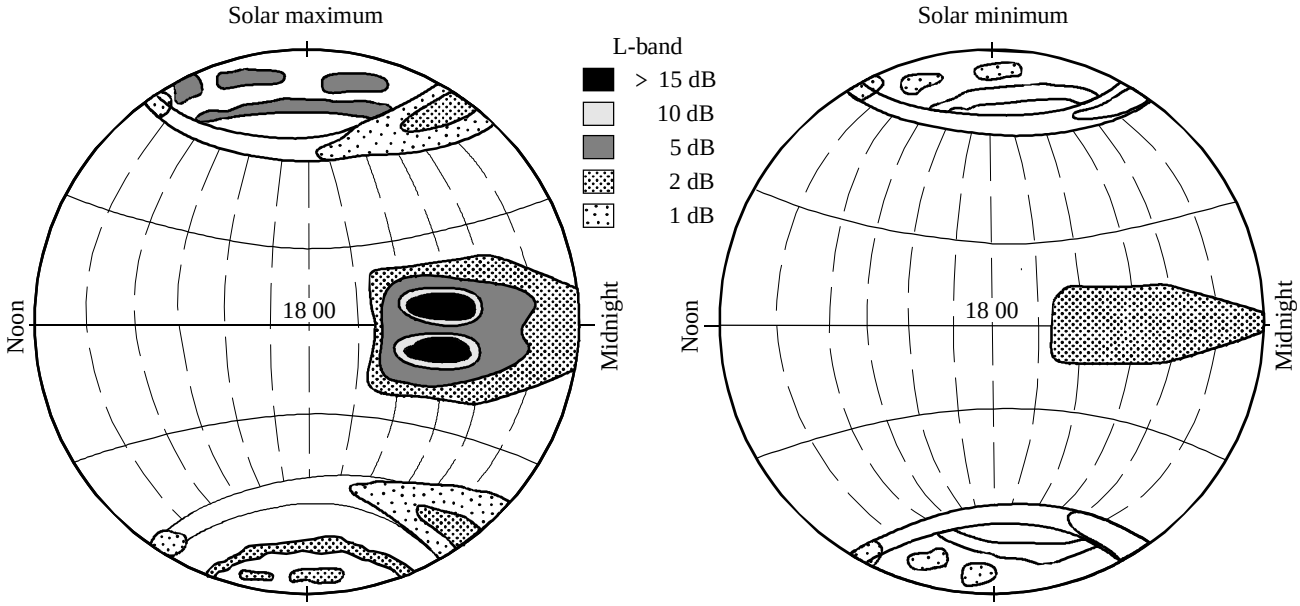

In terms of temporal characteristics, the fading rate of ionospheric scintillation is about 0.1 to 1 Hz. A typical scintillation event has its on-set after local ionospheric sunset and an event can last from 30 min to hours. For equatorial stations in years of solar maximum, ionospheric scintillation occurs almost every evening after sunset, with the peak-to-peak fluctuations of signal level at 4 GHz exceeding 10 dB in magnitude.

4.3 Instantaneous statistics and spectrum behaviour

4.3.1 Instantaneous statistics

During an ionospheric scintillation event, the Nakagami density function is believed to be adequately close for describing the statistics of the instantaneous variation of amplitude. The density function for the intensity of the signal is given by:

$$p(I) = \frac{m^m}{\Gamma(m)} I^{m-1} \exp(-mI) \tag{7}$$

where the Nakagami "*m*-coefficient" is related to the scintillation index, S_4 by:

$$m = 1 / S_4^2 \tag{8}$$

In formulating equation (7) the average intensity level of *I* is normalized to be 1.0. The calculation of the fraction of time that the signal is above or below a given threshold is greatly facilitated by the fact that the distribution function corresponding to the Nakagami density has a closed form expression which is given by:

$$P(I) = \int_0^I p(x)\,\mathrm{d}x = \frac{\Gamma(m, mI)}{\Gamma(m)} \tag{9}$$

where $\Gamma(m, mI)$ and $\Gamma(m)$ are the incomplete gamma function and gamma function, respectively. Using equation (9), it is possible to compute the fraction of time that the signal is above or below a given threshold during an ionospheric event. For example, the fraction of time that the signal is more than *X* dB below the mean is given by $P(10^{-X/10})$ and the fraction of time that the signal is more than *X* dB above the mean is given by $1 - P(10^{X/10})$.

4.3.2 Spectrum behaviour

Since ionospheric scintillations are believed to be caused by relatively stationary refractive-index irregularities moving horizontally past the radiowave path, the spatial and temporal power spectra are related by the drift velocity. The actual relationship depends on the irregularity composition (power spectra) and a number of other physical factors. As a result, the power spectra exhibit a wide range of slopes, from f^{-1} to f^{-6} as have been reported from different observations. A typical spectrum behaviour is shown in Fig. 6. The f^{-3} slope as shown is recommended for system applications if direct measurement results are not available.

4.4 Geometric consideration

4.4.1 Zenith angle dependence

In most models, S_4^2 is shown to be proportional to the secant of the zenith angle, *i*, of the propagation path. This relationship is believed to be valid up to $i \approx 70°$. At greater zenith angles, a dependence ranging between 1/2 and first power of sec *i* should be used.

4.4.2 Seasonal-longitudinal dependence

The occurrence of scintillations and magnitude of S_4 have a longitudinal as well as seasonal dependence that can be parameterized by the angle, β, shown in Fig. 7b. It is the angle between the sunset terminator and local magnetic meridian at the apex of the field line passing through the line-of-sight at the height of the irregularity slab. The weighting function for seasonal-longitudinal dependence is given by:

$$S_4 \propto \exp\left[-\frac{\beta}{W}\right] \tag{10}$$

where *W* is a weighting constant depending on location as well as calendar day of the year. As an example, using the data available from Tangua, Hong Kong and Kwajalein, the numerical value of the weighting constant can be modelled as shown in Fig. 8.

FIGURE 6

Power spectral density estimates for a geostationary satellite (Intelsat-IV) at 4 GHz

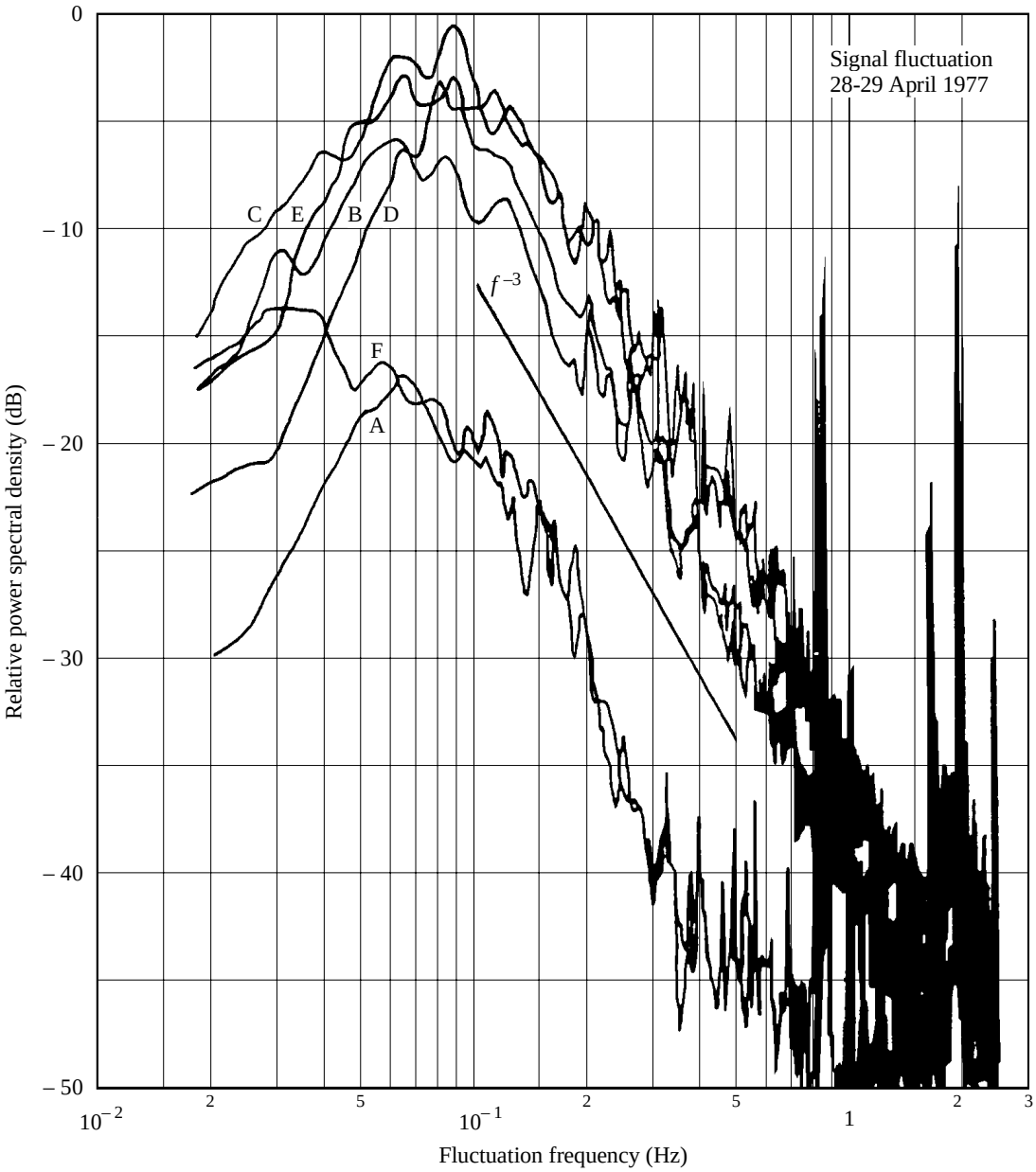

The scintillation event was observed during the evenings of 28-29 April 1977 at Taipei earth station

0531-06

A: 30 min before event onset
B: at the beginning
C: 1 h after
D: 2 h after
E: 3 h after
F: 4 h after

FIGURE 7a

Intersection of the propagation path with a magnetic field line at the F-region height

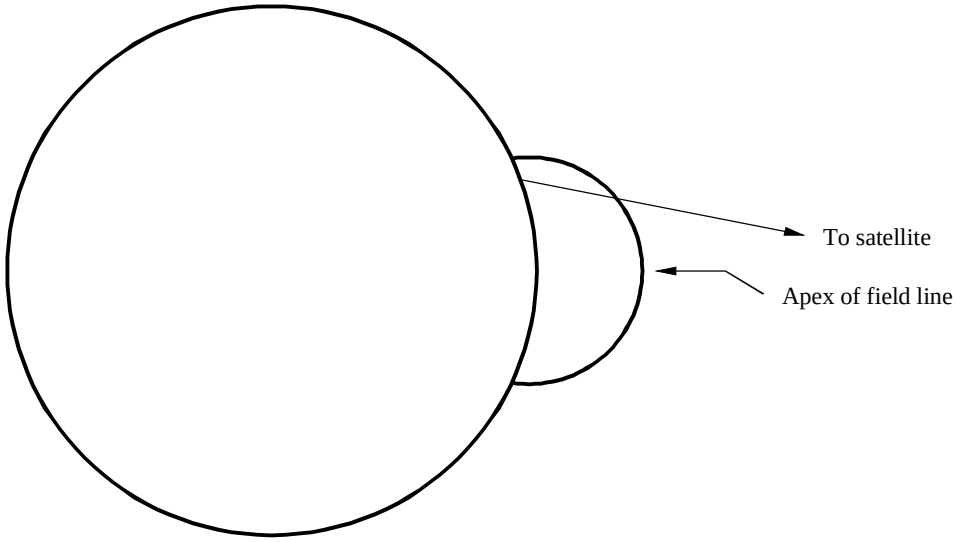

0531-07a

FIGURE 7b

Angle between the local magnetic meridian at the apex of the field line shown in Fig. 7a and the sunset terminator

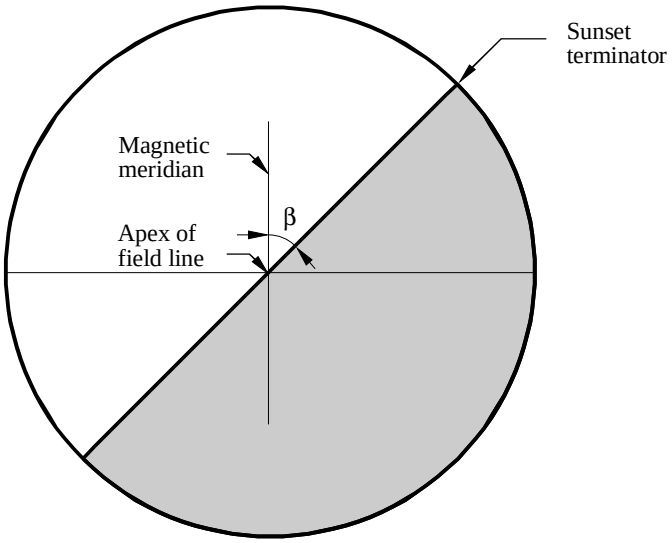

0531-07b

FIGURE 8

Seasonal weighting functions for stations in different longitude sectors

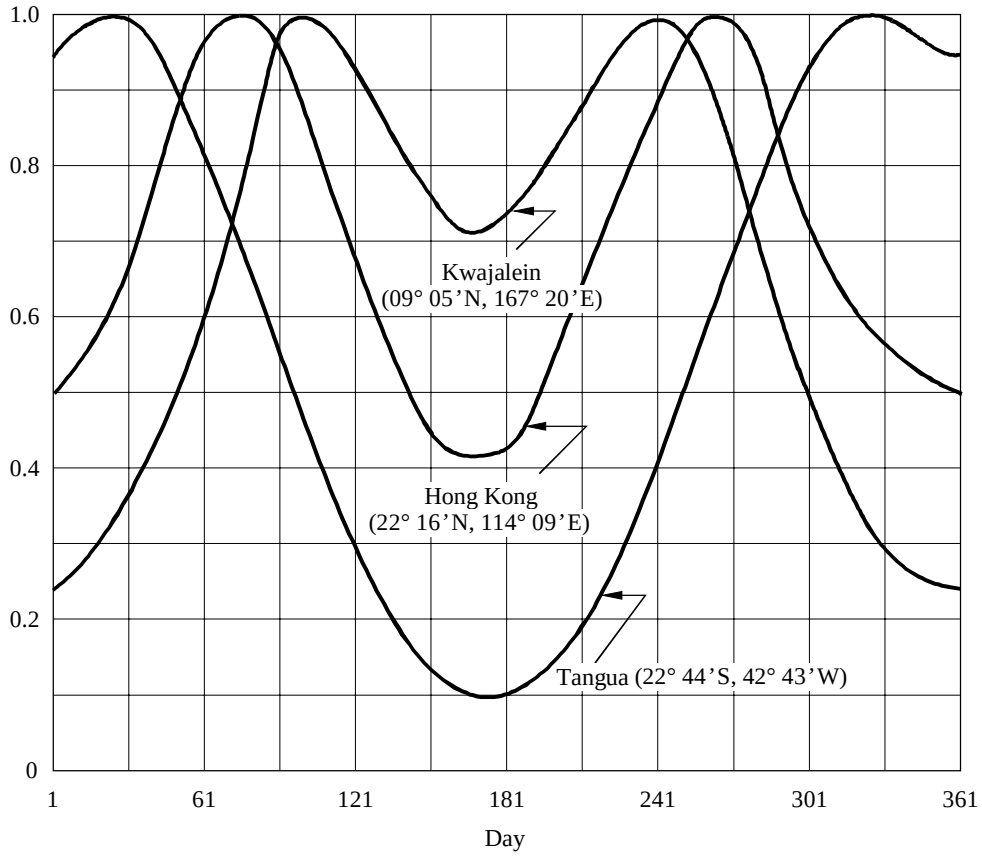

4.5 Cumulative statistics

When considering the design of satellite radiocommunication systems and the assessment of frequency sharing, communications engineers have concerns not only with the system degradation and interference during an event but also with the long term cumulative occurrence statistics. For communications systems involving a geostationary satellite, which is the simplest radio system configuration, Figs. 9 and 10 are recommended for the assessment and scaling of occurrence statistics. The sunspot numbers (SSN) cited are the 12 month averaged sunspot numbers.

FIGURE 9

Dependence of 4 GHz equatorial ionospheric scintillations on monthly mean sunspot number

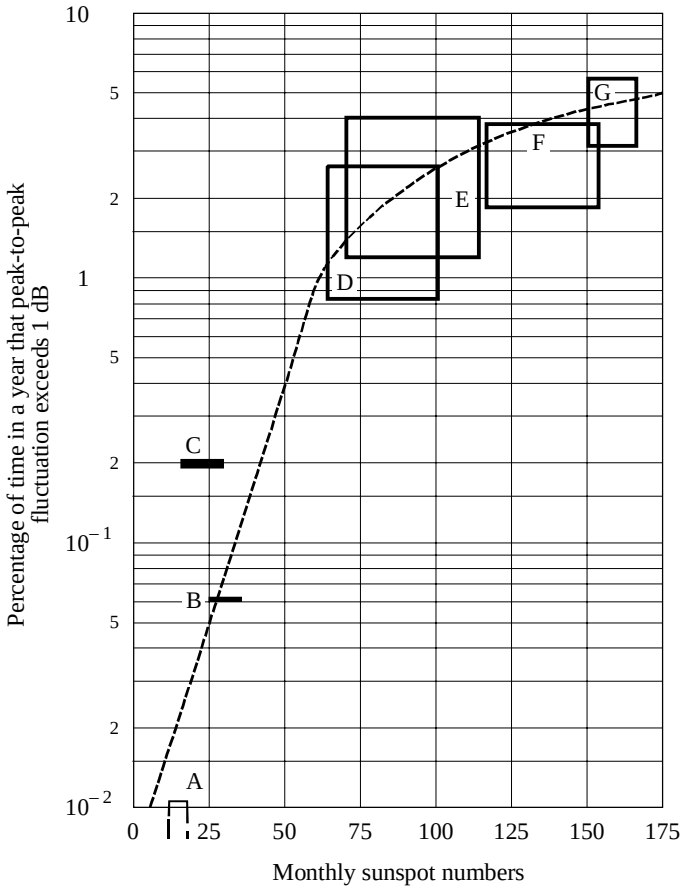

The squares are the ranges of variations over a year for different carriers

A: 1975-1976, Hong Kong and Bahrein, 15 carriers
B: 1974, Longovilo, 1 carrier
C: 1976-1977, Taipei, 2 carriers
D: 1970-1971, 12 stations, > 50 carriers
E: 1977-1978, Hong Kong, 12 carriers
F: 1978-1979, Hong Kong, 10 carriers
G: 1979-1980, Hong Kong, 6 carriers

0531-09

FIGURE 10

Annual statistics of peak-to-peak fluctuations observed at Hong Kong earth station (Curves I1, P1, I3-I6, P3-P6) and Taipei earth station (Curves P2 and I2)

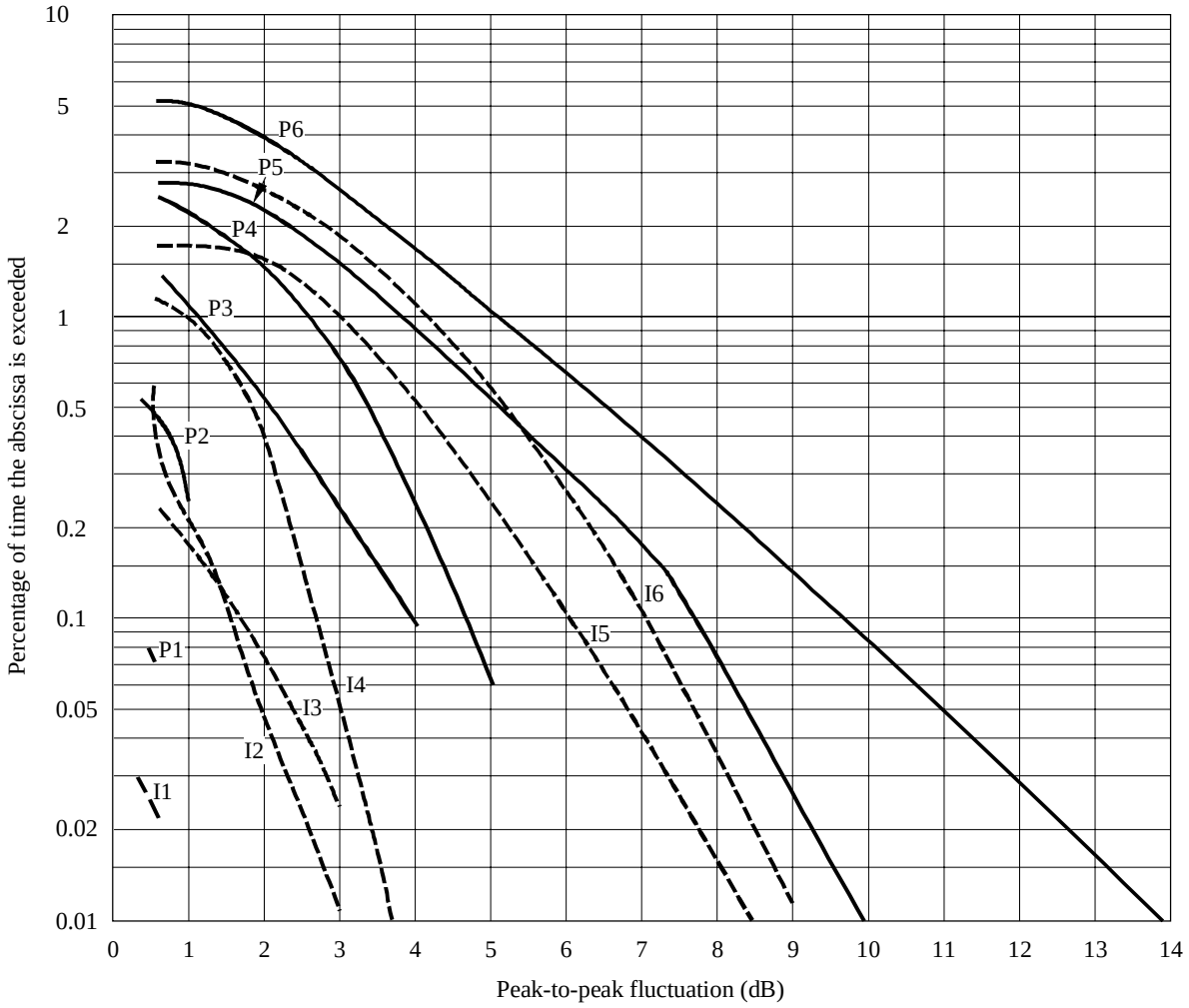

Curve	*Period*	*SSN range*
I1, P1	March 75-76	10-15
I2, P2	June 76-77	12-26
I3, P3	March 77-78	20-70
I4, P4	October 77-78	44-110
I5, P5	November 78-79	110-160
I6, P6	June 79-80	153-165

0531-10

The long-term cumulative distribution, $P(I)$, of the signal intensity relative to its mean value can be derived from the long-term cumulative statistics, F(ξ), of the peak-to-peak fluctuation, ξ, such as those found in Fig. 10, as follows:

$$P(I) = \sum_{i=0}^{n} f_i \, P_i(I) \tag{11}$$

where:

$$f_0 = \mathrm{F}(\xi < \xi_1) \tag{11a}$$

$$f_i = \mathrm{F}(\xi_i \leq \xi < \xi_{i+1}) \qquad (i = 1, 2, \ldots, n-1) \tag{11b}$$

$$f_n = \mathrm{F}(\xi \geq \xi_n) \tag{11c}$$

and ξ_1 and ξ_n are the minimum and maximum peak-to-peak fluctuation values, respectively, and n is the interval number of ξ of interest to the user;

$$P_i(I) = \Gamma(m_i, m_i I) / \Gamma(m_i) \tag{11d}$$

$$m_i = 1 / S_{4_i}^2 \tag{11e}$$

$$S_{40} = \left[\frac{1}{27.5} \cdot \frac{\xi_1}{2} \right]^{1/1.26} \tag{11f}$$

$$S_{4i} = \left[\frac{1}{27.5} \cdot \frac{\xi_i + \xi_{i+1}}{2} \right]^{1/1.26} \qquad (i = 1, 2, \ldots n-1) \tag{11g}$$

$$S_{4n} = \left[\frac{1}{27.5} \cdot \frac{\xi_{n-1} + 3\xi_n}{4} \right]^{1/1.26} \tag{11h}$$

Figure 11 shows an example of long-term cumulative distribution of signal intensity derived from the curve P6 of Fig. 10.

4.6 Simultaneous occurrence of ionospheric scintillation and rain fading

Ionospheric scintillation and rain fading are two impairments of completely different physical origin. However, in equatorial regions at years of high sunspot number, the simultaneous occurrence of the two effects may have an annual percentage time that is significant to system design. The cumulative simultaneous occurrence time was about 0.06% annually as noted at 4 GHz at Djutiluhar earth station in Indonesia. This value is unacceptably high for ISDN types of applications.

The simultaneous events have signatures that are often vastly different from those when only a single impairment, either scintillation or rain alone, is present. While ionospheric scintillation alone is not a depolarization phenomenon, and rain fading alone is not a signal fluctuation phenomenon, the simultaneous events produce a significant amount of signal fluctuations in the cross-polarization channel. Recognition of these simultaneous events is needed for applications to satellite-Earth radio systems which require high availability.

FIGURE 11

An example of long-term cumulative statistics of signal intensity (4 GHz, 20° elevation)

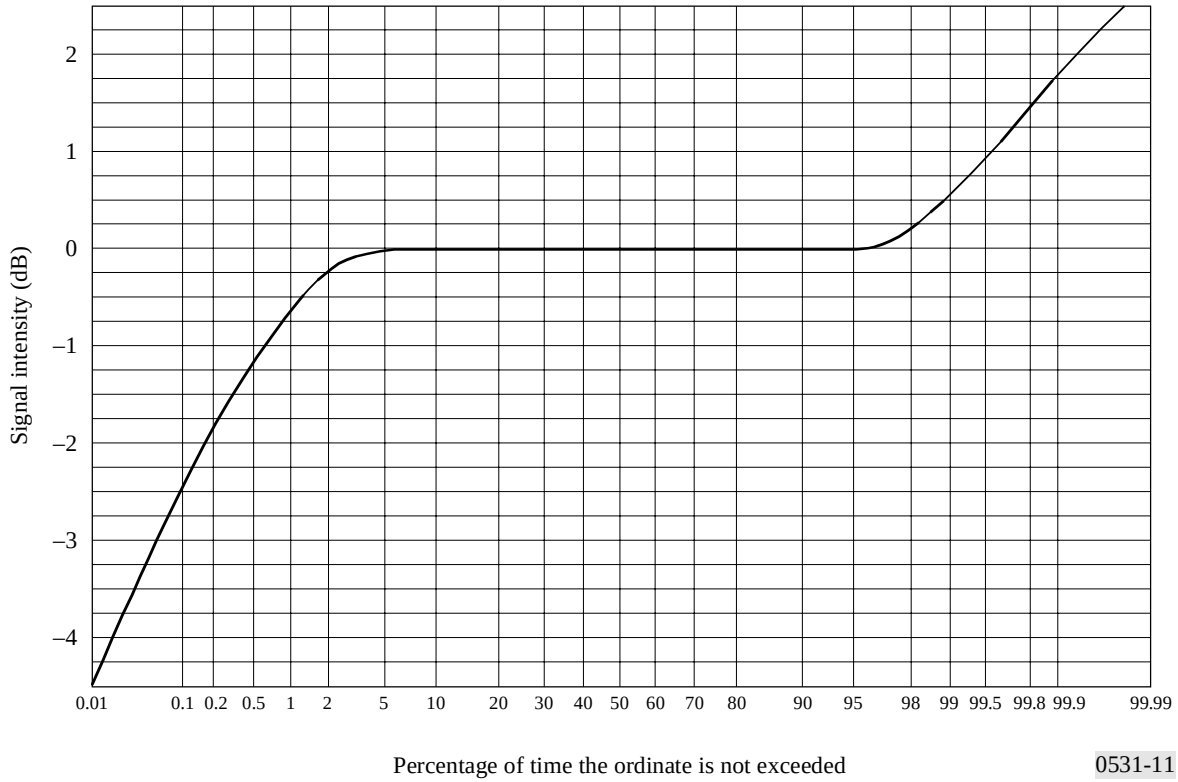

4.7 Gigahertz scintillation model

To evaluate the scintillation effects that can be expected in a given situation the following steps may be used:

Step 1: Figure 10 provides scintillation occurrence statistics on equatorial ionospheric paths: peak-to-peak amplitude fluctuations, P_{fluc}, (dB), for 4 GHz reception from satellites in the East at elevation angles of about 20° (P solid curves) and in the West at about 30° elevation (I dotted curves). The data are given for different times of year and sunspot number.

Step 2: Since Fig. 10 relates to 4 GHz, values for other frequencies are found by multiplying these values by $(f/4)^{-1.5}$ where f is the frequency of interest (GHz).

Step 3: The variation of P_{fluc} with geographical location and diurnal occurrence can be qualitatively estimated from Fig. 5.

Step 4: As one element of link budget calculations, P_{fluc} is related to signal loss L_p by $L_p = P_{fluc}/\sqrt{2}$.

Step 5: The scintillation index S_4, the most widely used parameter in describing scintillation, is defined in § 4.1 and may be obtained from P_{fluc} using Table 1.

5 Absorption

When direct information is not available, ionospheric absorption loss can be estimated from available models according to the $(\sec i)/f^2$ relationship for frequencies above 30 MHz, where i is the zenith angle of the propagation path in the ionosphere. For equatorial and mid-latitude regions, radiowaves of frequencies above 70 MHz will assure penetration of the ionosphere without significant absorption.

Measurements at middle latitudes indicate that, for a one-way traverse of the ionosphere at vertical incidence, the absorption at 30 MHz under normal conditions is typically 0.2 to 0.5 dB. During a solar flare, the absorption will increase but will be less than 5 dB. Enhanced absorption can occur at high latitudes due to polar cap and auroral events; these two phenomena occur at random intervals, last for different periods of time, and their effects are functions of the locations of the terminals and the elevation angle of the path. Therefore for the most effective system design these phenomena should be treated statistically bearing in mind that the durations for auroral absorption are of the order of hours and for polar cap absorption are of the order of days.

5.1 Auroral absorption

Auroral absorption results from increases of electron concentration in the D and E regions produced by incident energetic electrons. The absorption is observed over a range of 10° to 20° latitude centred close to the latitude of maximum occurrence of visual aurorae. It occurs as a series of discrete absorption enhancements each of relatively short duration, i.e. from minutes up to a few hours, with an average duration of about 30 min, and usually showing an irregular time structure. Night enhancements tend to consist of smooth fast rises and slow decays. Typical magnitudes at 127 MHz are shown in Table 2.

TABLE 2

Auroral absorption at 127 MHz (dB)

Percentage of the time	Angle of elevation	
	20°	5°
0.1	1.5	2.9
1	0.9	1.7
2	0.7	1.4
5	0.6	1.1
50	0.2	0.4

5.2 Polar cap absorption

Polar cap absorption which may occur at times of high solar activity, does so at geomagnetic latitudes greater than 64°. The absorption is produced by ionization at heights greater than about 30 km. It usually occurs in discrete, though sometimes overlapping, events which are nearly always associated with discrete solar events. The absorption is long-lasting and is detectable over the sunlit polar caps. Polar cap absorption occurs most usually during the peak of the sunspot cycle, when there may be 10 to 12 events per year. Such an event may last up to a few days. This is in contrast to auroral absorption, which is frequently quite localized, with variations in periods of minutes.

A remarkable feature of a polar cap absorption event is the great reduction in the absorption during hours of darkness for a given rate of electron production. Figure 12 is a hypothetical model of the diurnal variation of polar cap absorption following a major solar flare based upon riometer observations at various latitudes.

6 Summary

Table 3 estimates maximum values for ionospheric effects at a frequency of 1 GHz. It is assumed that the total vertical electron content of the ionosphere is 10^{18} el/m^2 column. An elevation angle of about 30° is also assumed. The values given are for the one-way traversal of the waves through the ionosphere.

FIGURE 12

Hypothetical model showing polar cap absorption following a major solar flare as expected to be observed on riometers at appproximately 30 MHz

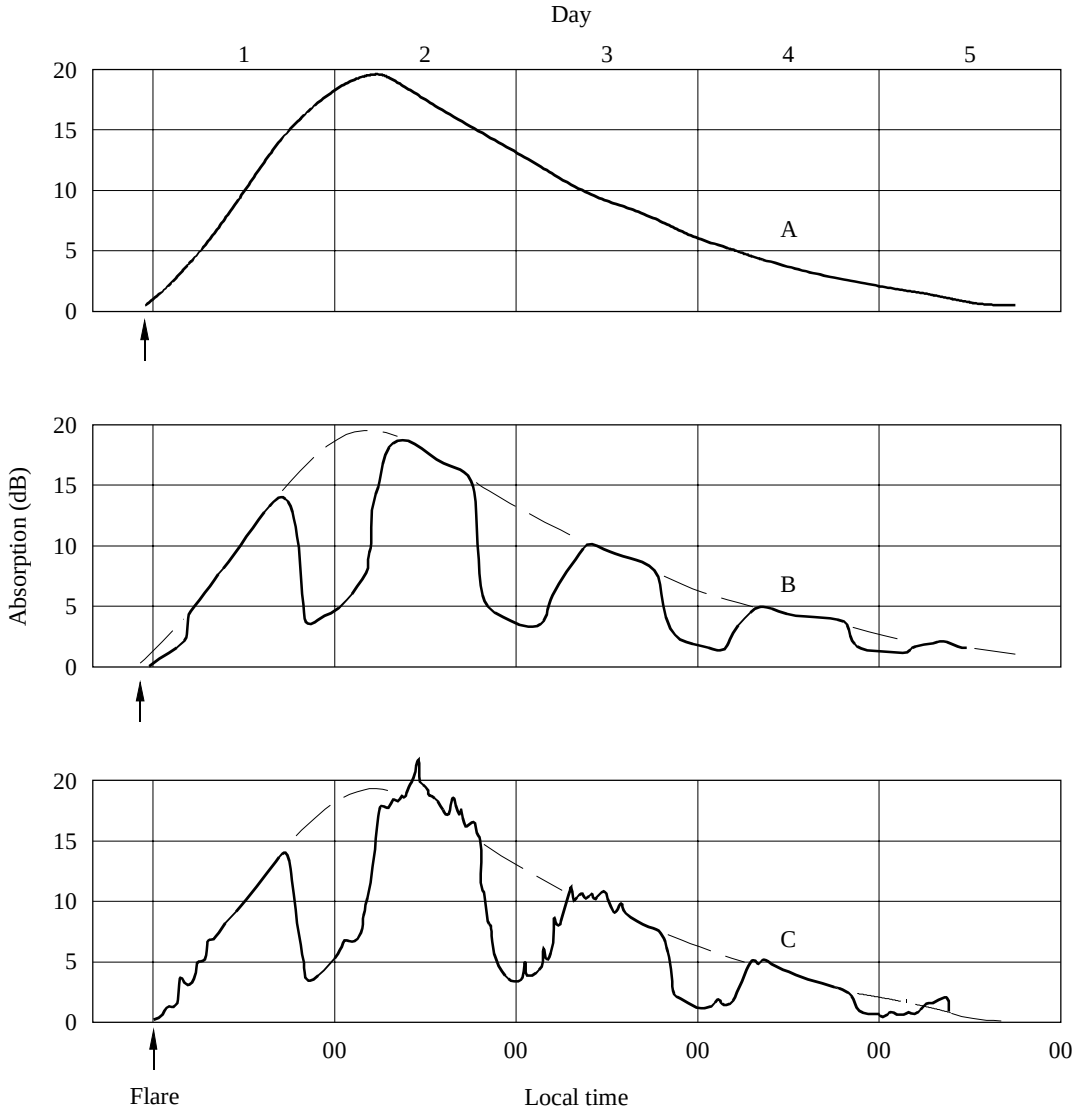

A: high latitudes – 24 h of daylight
B: high latitudes – equal period of day and night
C: high latitudes – auroral zone

0531-12

TABLEAU 3

Estimated maximum ionospheric effects at 1 GHz for elevation angles of about 30° one-way traversal

Effect	Magnitude	Frequency dependence
Faraday rotation	108°	$1/f^2$
Propagation delay	0.25 μs	$1/f^2$
Refraction	< 0.17 mrad	$1/f^2$
Variation in the direction of arrival	0.2 min of arc	$1/f^2$
Absorption (polar cap absorption)	0.04 dB	~$1/f^2$
Absorption (auroral + polar cap absorption)	0.05 dB	~$1/f^2$
Absorption (mid-latitude)	< 0.01 dB	$1/f^2$
Dispersion	0-4 ns/MHz	$1/f^3$
Scintillation	See § 4	See § 4